Precise CP violation measurement in the ATLAS experiment at the CERN LHC

M. Melcher

Precise CP violation measurement in the ATLAS experiment at the CERN LHC

Martin Melcher

Maîtrise at the University Joseph Fourier of Grenoble

Project supervisor: Faïrouz Ohlsson-Malek

Institut des Sciences Nucléaires de Grenoble

June 2001

Acknowledgements

I would like to thank the laboratory for having accomodated me, permitting me to get an impression of the scientist's everyday life and to work on an interesting subject. I specially thank my project supervisor Faïrouz Ohlsson-Malek for her guidance and patience.

Thanks go furthermore to the members of the ATLAS group I worked with for their help and for having contributed to a very motivating work atmosphere.

Very special thanks to David Rousseau from LAL-Orsay, who read all my report and gave constructive commentaries and hints.

Then, thanks to Edwige Tournefier, Sophia Saboumazrag, Sébastien Viret and Ulrich Meier for their friendly help and accompany.

Last but not least I would like to thank Dieter Engelhardt from the University of Karlsruhe for his engagement and for having encouraged me with his enthusiastic speeches to stay a year in France.

Contents

1 Introduction

Driven by curiosity, man always wanted to know and understand the basic principles of what he sees in the world around him. Pushed by the need to understand, he started to construct increasingly large experiments in order to force nature to show its laws. Among the most recent ones, we find the big particle accelerators, which can be seen as huge microscopes, and which already lead to a deeper understanding of the basic bricks of the universe, the elementary particles. What was observed found an explanation in a theory called the *standard model*, able to describe in astonishing precision the world at smallest scale.

Nevertheless, one of the most fundamental questions could not yet be answered: Where does matter come from? In all processes observed, exactly the same amounts of matter and antimatter are created or destroyed, while it seems that our universe contains practically no antimatter. What happened to it? Small differences between the behaviour of matter and antimatter were found, a basic symmetry called CP seems to be violated. Hoping this could lead to an explanation, this CP symmetry violation is to be investigated.

Special interest is driven to B meson decays, as they are concerned by CP violation and permit to investigate in detail several of its aspects and properties. One of the most important tools involved will be the **L**arge **H**adron **C**ollider which is in this moment under construction at CERN in Geneva. In the high-energetic proton-proton-collisions at LHC, large amounts of B mesons will be created and hopefully detected and investigated by, among others, the ATLAS detector, an all-purpose particle detection and identification system. By this, the parameters controlling CP violation as described in the theory can be measured precisely, and perhaps even new physics beyond the standard model is found.

In order to know if this investigations will be possible, the capability of the ATLAS detector to 'see' B meson decays was explorated by numerical simulations. This was the subject of the work presented here, where two selected B decay modes, $B_s \to J/\psi\ \eta$ and $B_d \to J/\psi\ K^{*0}$ were analyzed. Using data from simulation, the decay products were searched for, identified and combined, in order to reconstruct the B mesons at the end. By this, estimates on the number of B mesons which will be observed in ATLAS and on the cleanliness of the signal can be given.

2 Short presentation of the laboratory

2.1 ISN Grenoble

The institute for nuclear science (ISN) is a mixed laboratory for fundamental research in the domain of subatomic physics, under supervision of the national center of scientific research (CNRS) and the national institut of nuclear and particle physics (IN2P3) on the one hand, and the university Joseph Fourier (UJF) on the other hand.

The domain of scientific research is divided into three experimental and theoretical subdomains, corresponding to increasingly fine scales of matter and increasingly high energies of the accelerators:

- Nuclear and hadronic matter
- Particle physics
- Astroparticle physics

Participating to international collaborations, and with the help of engineers and technicians, the physicists design and construct modules for complex detectors, such as ATLAS at CERN.

The ISN was founded in 1966 and employs at the moment ca. 200 scientists, engineers and technicians, as well as students and foreign guests.

2.2 CERN Geneva

Founded in 1954 by 12 member states, CERN, the european laboratory for particle physics, has become the world largest center for particle physics research. It counts 20 member states at the moment, and 7000 particle physicists, half of all the particle physicists of the world, use the installations of CERN, representing 500 universities and 80 nationalities.

Being dedicated to particle physics at highest energies, the principal activities at CERN concern the accelerators, the largest of wich was LEP, a circular accelerator measuring a circumference of 27 km. In order to achieve even higher energies, it is at this moment being replaced by LHC, a proton-proton collider at 14 TeV center-of-mass energy, which will start work in 2005.

3 The standard model

3.1 Introduction

The standard model is the reference theory in particle physics, fully accepted by the physics community. Being based on fundamental symmetries (and their breaking) and perturbative quantum field theory, it is able not only to explain the observations being made, but also to make quantitative predictions, which were verified by experiments up to extraordinary precisions.

Yet, the standard model does not include gravity, and it is based on 21 free parameters, which have to be derived from experiment. This is why its limits have to be explored, in order to find new physics "beyond the standard model", hopefully leading to a more fundamental theory.

3.2 Some basics

In the standard model, interactions between the elementary particles are described as exchange of virtual gauge bosons, particles, which appear and disappear without being directly observed.

All of the four fundamental forces have their proper gauge bosons - For the electromagnetic force it is the well-known photon, for the strong nuclear force the gluon and for the weak force the $W^{\pm}$ and Z^0 bosons. The possible interactions find their visualisation in the famous Feynman-graphs, some examples of which are shown in figure 1.

In the perturbative approach, one takes advantage of the fact that an interaction route becomes less probable, if more interactions are involved. For

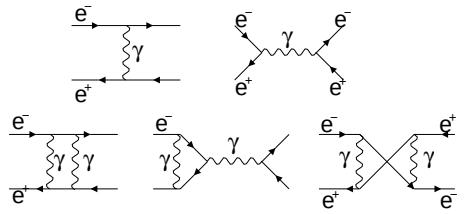

Figure 1: Some second (leading) and fourth order contributions to $e^+ - e^-$-scattering

this reason, the process can be calculated using only the most simple Feynman-graphs. An amplitude is associated to each Feynman-graph - consisting of the probability of the represented interaction route and a complex phase. In order to get the overall probability of the process, the amplitudes of all contributing Feynman-graphs (all graphs having the same 'input' and 'output') have to be summed up. This leads to interference phenomena, as several contributions fully or partially annihilate or enhance themselves due to the complex phases.

Since it was proven by E. Noether that there is a conserved quantity associated to each symmetry, the search for symmetries has become a fundamental part of the physicists work. And even if a symmetry is (totally or partially) broken, it can still provide valuable information. An overview of the the fundamental symmetry operations if given in appendix A.

3.3 Kaon systems and CP violation

Neutral K mesons, being composed of a strange and a down quark, show some interesting properties due to flavour mixing and lead to the first discovery of CP violation in 1964.

While the mass eigenstates are the usual K meson $\left|K^0\right\rangle$ and its antiparticle $\left|\overline{K^0}\right\rangle$, it appeared that the states seen by weak interaction, the weak eigenstates, are the linear combinations $|K_1\rangle = \frac{1}{\sqrt{2}}\left(\left|K^0\right\rangle - \left|\overline{K^0}\right\rangle\right)$ and $|K_2\rangle = \frac{1}{\sqrt{2}}\left(\left|K^0\right\rangle + \left|\overline{K^0}\right\rangle\right)$, which are CP eigenstates, as $CP\,|K_1\rangle = +\,|K_1\rangle$ and $CP\,|K_2\rangle = -\,|K_2\rangle$. As illustrated in Figure 2, this behaviour is very similar to the behaviour of two coupled pendulums, the free oscillations of which are linear combinations of the oscillations of each pendulum alone.

The K_1 and K_2 components decay with different decay widths into different endstates, which are also CP eigenstates:

$$\begin{array}{lcllll|l} K_1 & \rightarrow & \pi^+\pi^- & or & \pi^0\pi^0 & & CP = +1 \\ K_2 & \rightarrow & \pi^+\pi^-\pi^0 & or & \pi^0\pi^0\pi^0 & & CP = -1 \end{array} \qquad (1)$$

In 1964, also $K_2 \rightarrow 2\pi$ decays were observed, which would be forbidden if CP was conserved. It was found that the weak eigenstates are not, as assumed, equal mixtures of K^0 and $\overline{K^0}$, but:

$$\left|K_S^0\right\rangle = \frac{1}{\sqrt{1+\epsilon^2}}\left(\left|K_1\right\rangle + \epsilon \cdot \left|K_2\right\rangle\right) \text{ and } \left|K_L^0\right\rangle = \frac{1}{\sqrt{1+\epsilon^2}}\left(\left|K_2\right\rangle - \epsilon \cdot \left|K_1\right\rangle\right) \quad (2)$$

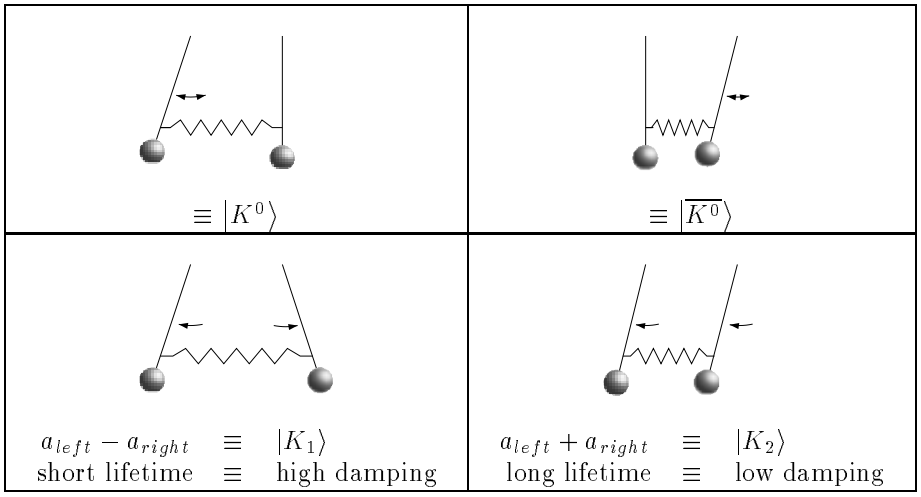

Figure 2: Kaon weak eigenstates and mechanical analogon

where $\epsilon \approx 2 \cdot 10^{-3}$ quantizes the CP violation. In fact, the K_S^0 component is slightly dominated by the particle K^0, whereas K_L^0 is dominated by the antiparticle $\overline{K^0}$.

3.4 CP violation in the standard model

3.4.1 Types and mechanisms of CP violation

Although the standard model itself does not predict CP violation, a theoretical description was derived within this framework, introducing new parameters wich have to be obtained by experiments. Only the weak force is concerned by CP violation.

CP violation effects can be classified into two categories:

- **Direct CP violation.** In this case, the decay rate for a decay $A \to B$ differs from its CP conjugate, $\bar{A} \to \bar{B}$. This requires that there are two different decay routes, as indicated in figure 3, with different phases, wich interfere.

- **Indirect/mixing-induced CP violation.** This is the case if, as in the $K^0 - \overline{K^0}$ system, processes that change the particle into its antiparticle $\left(A \to \bar{A}\right)$ are accessible, leading to weak eigenstates which are linear combinations of mass eigenstates. Consequently, the decay routes $A \to B$ and $A \to \bar{A} \to B$ (a) can interfere, as well as $\bar{A} \to B$ and $\bar{A} \to A \to B$ (b). If furthermore the final state B is a CP eigenstate, then the decay (b) is the CP-conjugate of (a). Hence, if, due to complex phases, the decay amplitudes of (a) and (b) are different, CP is violated.

3.4.2 CKM matrix and unitarity triangles

In order to connect the weak eigenstates (d', s', b') of the down, strange and bottom quark with their mass eigenstates (d, s, b), the Cabibbo-Kobayashi-Maskawa

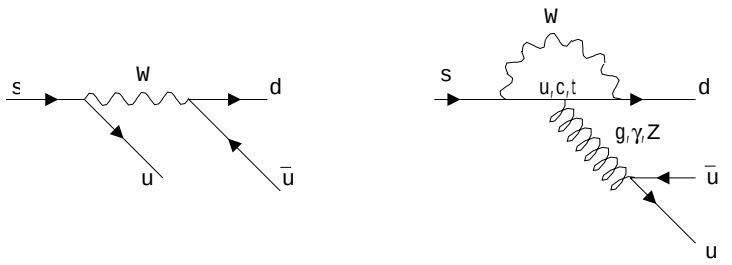

Figure 3: Tree (left) and penguin contributions to s quark decays

(CKM) matrix was introduced:

$$\begin{pmatrix} d' \\ s' \\ b' \end{pmatrix} = \begin{pmatrix} V_{ud} & V_{us} & V_{ub} \\ V_{cd} & V_{cs} & V_{cb} \\ V_{td} & V_{ts} & V_{tb} \end{pmatrix} \cdot \begin{pmatrix} d \\ s \\ b \end{pmatrix} \equiv \hat{V}_{CKM} \cdot \begin{pmatrix} d \\ s \\ b \end{pmatrix} \tag{3}$$

The CKM-matrix is unitary:

$$\hat{V}_{CKM}^{\dagger} \cdot \hat{V}_{CKM} = \hat{1} = \hat{V}_{CKM} \cdot \hat{V}_{CKM}^{\dagger} \tag{4}$$

It can be parametrized by a phenomenological expansion in powers of the small quantity $\lambda \equiv |V_{us}| \approx 0.22$. This 'Wolfenstein parametrization' turns out to be quite useful:

$$\hat{V}_{CKM} = \begin{pmatrix} 1 - \frac{1}{2}\lambda^2 & \lambda & A\lambda^3(\rho - i\eta) \\ -\lambda & 1 - \frac{1}{2}\lambda^2 & A\lambda^2 \\ A\lambda^3(1 - \rho - i\eta) & -A\lambda^2 & 1 \end{pmatrix} + \mathcal{O}(\lambda^4) \tag{5}$$

CP violation is closely related to the parameter $\rho + i\eta$.

The unitarity of the CKM-matrix implies a set of 6 normalization and 6 orthogonality equations. The latter can be represented as 6 triangles in the complex plane. However, in only two of them, the three sides are of comparable magnitude $\mathcal{O}(\lambda^3)$, while in the others, one side is suppressed relative to the others. B physics is governed by the two non-squashed triangles, whereas the Kaon complex is related to a triangle where the sides don't have the same order of magnitude:

$$\left.\begin{array}{ccccccc} \overbrace{V_{ud}^* V_{us}}^{\mathcal{O}(\lambda)} & + & \overbrace{V_{cd}^* V_{cs}}^{\mathcal{O}(\lambda)} & + & \overbrace{V_{td}^* V_{ts}}^{\mathcal{O}(\lambda^5)} & = 0 \end{array}\right\} \text{K mesons} \tag{6}$$

$$\left.\begin{array}{ccccccc} V_{ud}V_{ub}^* & + & V_{cd}V_{cb}^* & + & V_{td}V_{tb}^* & = 0 \\ \underbrace{V_{ud}^* V_{td}}_{\mathcal{O}(\lambda^3)} & + & \underbrace{V_{us}^* V_{ts}}_{\mathcal{O}(\lambda^3)} & + & \underbrace{V_{ub}^* V_{tb}}_{\mathcal{O}(\lambda^3)} & = 0 \end{array}\right\} \text{B mesons} \tag{7}$$

The last two relations are represented in figure 4, where

$$\bar{\rho} \equiv \left(1 - \frac{\lambda^2}{2}\right)\rho, \;\; \bar{\eta} \equiv \left(1 - \frac{\lambda^2}{2}\right)\eta \tag{8}$$

It is to note that this two unitarity triangles are identical up to $\mathcal{O}(\lambda^3)$ and can only be distinguished by precision measurements which will take place in the near future.

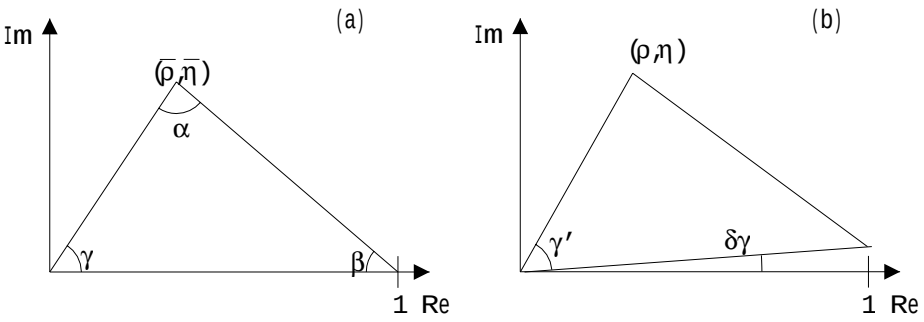

Figure 4: The two non-squashed unitarity triangles, where (a) corresponds to the first relation in (7) and (b) to the second.

3.5 B physics and time dependant CP violation

Yet, CP violation was only observed in Kaon systems. However, much larger effects are expected in neutral B meson decays. Additionally, B_s and B_d decays will permit to measure the angles of the unitarity triangles.

In case the final state of the decay to be analyzed is a CP eigenstate f_{CP}, these measurements can take place by comparing the following two decay widths:

- $\Gamma(t)$: The B meson is created as B^0 at time $t = 0$. Due to B oscillations $B^0 \leftrightarrow \overline{B^0}$, the two decay routes $B^0 \to f_{CP}$ and $B^0 \to \overline{B^0} \to f_{CP}$ interfere.
- $\overline{\Gamma}(t)$: The B meson is created as $\overline{B^0}$ at time $t = 0$. Due to B oscillations $B^0 \leftrightarrow \overline{B^0}$, the two decay routes $\overline{B^0} \to f_{CP}$ and $\overline{B^0} \to B^0 \to f_{CP}$ interfere.

Here, B^0 stands for a B_s or B_d meson. The resulting time-dependant CP asymmetry can be expressed as

$$a_{CP}(t) = \frac{\Gamma(t) - \overline{\Gamma}(t)}{\Gamma(t) + \overline{\Gamma}(t)} = \mathcal{A}_{CP}^{dir} \cos(\Delta M t) + \mathcal{A}_{CP}^{mix} \sin(\Delta M t) \tag{9}$$

where ΔM is the mass difference between the two mass eigenstates of the $B^0 - \overline{B^0}$-system. $\mathcal{A}_{CP}^{dir}$ is the contribution of direct CP violation, only present if the decay amplitude is the result of interference of a tree-style and a penguin-style decay route. If the decay is dominated by only one route, only the mixing-induced part $\mathcal{A}_{CP}^{mix}$ contributes. It can be expressed as

$$\mathcal{A}_{CP}^{mix} = \eta_{f_{CP}} \sin(\phi_{f_{CP}}) \tag{10}$$

where $\eta_{f_{CP}}$ is the CP parity (eigenvalue) of the final state f_{CP} and $\phi_{f_{CP}}$ the phase of a certain product of CKM elements, depending on the final state. In the case of $B_d \to J/\psi\ K^{*0}$, for example, we get the simple relation $\phi_{f_{CP}} = 2\beta$, where β is one of the angles of the unitarity triangle as shown in figure 4. Therefore, this mode permits a clean measurement of this angle.

Different methods to decide wether the B meson was born as B^0 or $\overline{B^0}$ are presented in [2, chapter 2.7].

4 LHC and ATLAS

4.1 LHC

LHC, currently under construction, will be a proton-proton collider providing 14 TeV center-of-mass energy. The protons will be accelerated in a synchrotron with a circumference of 27 km.

The luminosity $\mathcal{L}$ is defined so that $\mathcal{L} \cdot \sigma$ gives the number of reactions per second, where σ is the cross section of the reaction. During the first three years, it will be at $\mathcal{L} = 10^{33} cm^{-2} s^{-1}$ (low luminosity run); thereafter it will be rised to $\mathcal{L} = 10^{34} cm^{-2} s^{-1}$ (high luminosity run).

The colliding protons are accumulated in bunches, and many bunches are stored in the accelerator ring at the same time. Hence, the collisions do not happen continuously, but only during the bunch crossings.

As LHC is a hadronic machine colliding protons, which are themselves composed of three quarks each, one will have to deal with large amounts of hadronic jets, events which will be uninteresting for the analysis here and which can be seen as noise. Therefore, one of the main tasks will be to identify and reject this hadronic jets.

In order to describe the reactions taking place at the interaction points, usually a coordinate system consisting of the coordinate z (along the beam axis), the angle ϕ and the pseudorapitidy η is used (see appendix C).

4.2 The ATLAS detector

ATLAS is one of the four detectors which will analyze the results of the collisions at four different interaction points. It is an all-purpose particle detection and identification system, providing facilities to detect and measure a maximum of all particles. As shown in figure 5, it is composed of several layers, which are, beginning with the innermost one:

- The **inner detector**. In this section, particle tracks are detected by semiconductor subdetectors, permitting high precision vertexing. The inner detector is contained in a high magnetic field, bending the tracks of charged particles. Measuring the bending radius will permit to calculate the particles momenta.
- The **electromagnetic calorimeter** (ECAL). Being itself composed of several layers, which will be explained in more detail in the following section, this section is designed to absorb electromagetic particles (photons, electrons, positrons) and measure the amounts of energy being deposited by the particles.
- The **hadronic calorimeter** (HCAL). This section is designed to absorb hadronic particles, which will deposit only a small amout of energy in the ECAL, as they are heavier and are not stopped as easily as photons and electrons.
- The **muon chambers**. The only particles being able to pass trough the electromagnetic and hadronic calorimeters are, besides neutrinos, which cannot be detected, muons. They are detected by the outermost layer, the muon chambers, where they can easily be identified.

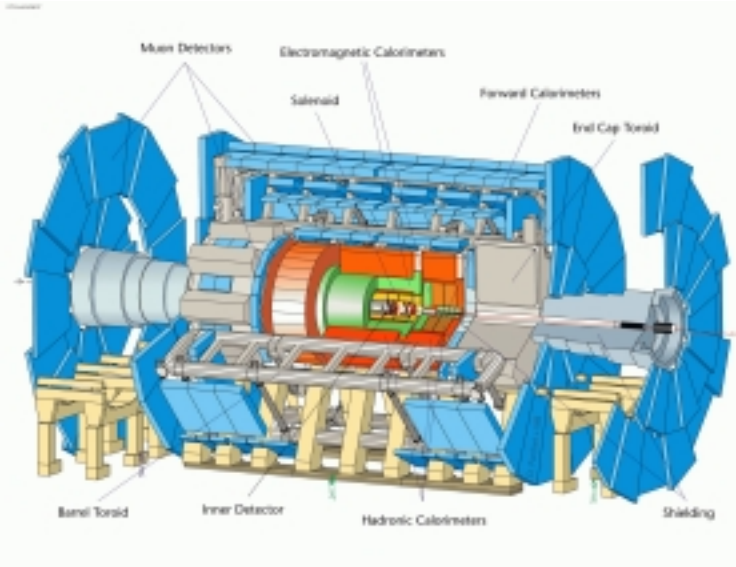

Figure 5: Schematig view of the ATLAS detector

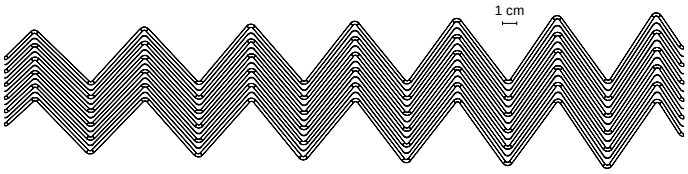

Figure 6: Accordion structure of the ECAL

4.3 A closer look at the electromagnetic calorimeter

The ECAL is the most important part of the detector for photon reconstruction, as photons are not seen in the inner detector and deposit nearly all of their energy in the ECAL.

It is composed of lead absorber plates and liquid-argon detector plates, organized in an accordion structure as shown in figure 6.

It is subdivided into the following sections:

- The **presampler.** In the regions where the particles have to pass trough much material before reaching the ECAL, the presampler compensates for the energy losses.
- **First sampling.** This section consists of fine strips, giving a very high resolution in η direction, but a rather coarse one in ϕ direction. Due to the high η resolution, the first sampling permits to analyze the substructure of electromagnetic clusters.
- **Second sampling.** In this region, most of the energy is deposited. The second sampling consists of square towers, providing good resolution in both η and ϕ direction.

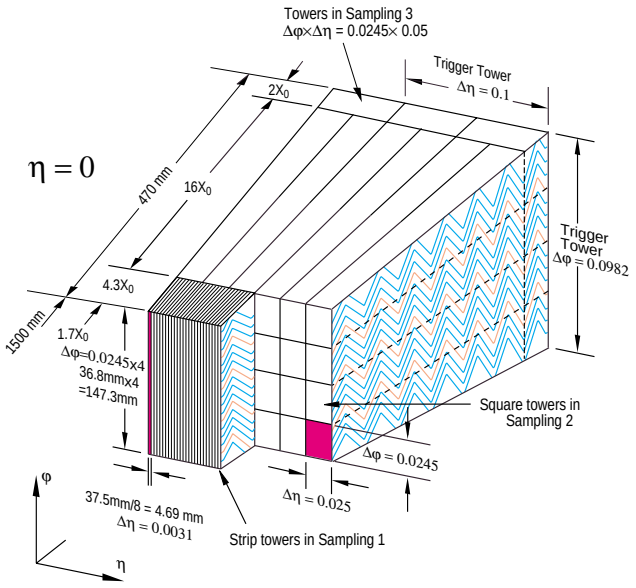

Figure 7: Granularity of the ECAL

- **Third sampling.** The η resolution of this region is twice coarser than the resolution in second sampling. This is sufficient for the physics requirements (jet reconstruction and measurement of missing transverse energy).

The alignment and resolution of the different parties are shown in figure 7.

The barrel segment of the ECAL covers the pseudorapidity region $|\eta| < 1.475$, whereas the endcap segments cover $1.375 < |\eta| < 3.2$.

4.4 Electromagnetic clusters

If an electron, positron or photon enters the calorimeter, it looses its energy by creating lots of new particles: e^+/e^--pairs, bremsstrahlung and other effects lead to an avalanche of particles, until the energy of the particles is too low for further particle creation. At the end, all the energy of the particle is deposited in the calorimeter. The ECAL is constructed so that the resolution is finer than the typical cluster width, which permits measurements on the cross section and inner structure of the clusters.

4.5 Reconstruction

As the energy of an electromagnetic cluster is distributed over a region of the ECAL, an algorithm is needed which relates the energy deposition of neighboured ECAL regions in order to find energy depositions belonging to the same cluster.

The chosen algorithm uses a virtual 3x3 tower window which is moved all over the ECAL, until the total energy deposited in this nine towers is above $1\ GeV$. In this case, it is assumend that the energy deposition belongs to an electromagnetic shower, and its properties (energy distribution, cluster width,

total energy etc.) is calculated, taking into account also the towers outside the 3x3 window.

4.6 Electronic noise and pile-up

Noise in the cables and read-out electronics gives birth to phantom clusters which have to be eliminated by each reconstruction algorithm. As the energy threshold used in the clusterization algorithm presented above is at 1 GeV, a lage amount of e-noise is already rejected.

The second problem arises from the fact that the read-out electronic is much slower than the reaction rate. In fact, the time needed for one readout exceeds the time of a bunch crossing. Therefore, each recorded event is the result of a superimposition of many reactions. At low luminosity, it is expected that in mean approx. 23 'minimum-bias' events, events, which will be observed by the detector and therefore cause noise, are superimposed. This superimposition effect is called pile-up. Pile-up consists mainly of hadronic clusters, coming from pions and other particles.

As also the electronic noise is accumulated, also phantom clusters above 1 GeV will be found.

B physics will be possible only at low luminosity, because the pile-up noise is too high for accurate analysis at high luminosity. Hence, all analysis were made at low luminosity.

5 Reconstructing $B_s \to J/\psi\ \eta$ and $B_d \to J/\psi\ K^{*0}$

5.1 Motivation

5.1.1 Interest in $B_s \to J/\psi\ \eta$

In analogy to the 'gold-plated' mode $B_s \to J/\psi\ \phi$, this decay channel permits to measure the angles γ and $\delta\gamma$ of the unitarity triangles, allowing to determine the parameter η in the Wolfenstein parametrization (5). As the angle $\delta\gamma$ is small, this mode represents a sensitive probe for CP-violating contributions beyond the standard model.

The difference to the decay in $J/\psi\ \phi$ is that the endstate $J/\psi\ \eta$ is a CP eigenstate. Therefore, no further analysis is needed in order to disentangle the CP odd and even parties of the endstate.

Experimentally, this mode is interesting because the J/ψ particle decays into $\mu^+\mu^-$ with a branching ratio of 5.88% [6]. The muons are easily identified in the muon chambers and reconstructed in the inner detector, permitting a very efficient J/ψ reconstruction, as was done in [5]. The η particle decays into $\gamma\gamma$ with a branching ratio of 39.3% [6], permitting a detection in the electromagnetic calorimeter.

5.1.2 Interest in $B_d \to J/\psi\ K^{*0}$

This mode permits a clean measurement of the parameter $\sin(2\beta)$, similar to the gold-plated mode $B_d \to J/\psi\ K_s$.

The advantage of the $J/\psi\ K^{*0}$ mode is the comparatively high branching rate ($1.58 \pm 0.27 \cdot 10^{-3}$ in comparison to $8.9 \pm 1.2 \cdot 10^{-4}$ for the $J/\psi\ K_s$ decay

[6]). In addition, the results from CLEO and CDF indicate that the state $J/\psi\ K^{*0}$ is dominated by CP-even states, for its P wave component is very small [11]. Therefore, no further analysis for CP odd/even state separation is needed, either.

According to standard model predictions, only mixing-induced CP violation will contribute, whereas the direct CP violation will be negligible. Hence, the discovery of direct CP violation in this decay mode would also lead to new physics beyond the standard model.

5.2 Simulation

For the analysis, the reactions themselves and their impact on the ATLAS detector were simulated, taking into account all known physical effects. A more detailed description of the simulation step is given in appendix D.

The exclusive modes $B_s \to J/\psi\ \eta$ and $B_d \to J/\psi\ K^{*0}$ were analyzed using two different data samples. At the generation level, the following decays were forced: $J/\psi \to \mu^+\mu^-$, $\eta \to \gamma\gamma$, $K^{*0} \to K^0 X$, $K^0 \to K_s^0 \to \pi^+\pi^-$. The $K^{*0} \to K^0\pi^0$ branching rate is next to 100%, but with a probability of 0.23%, also $K^{*0} \to K^0\gamma$ is found [6]. This was taken into account in the data sample. Furthermore, the cuts $|\eta| < 2.5$, $p_T(\mu) > 6\ GeV$ were applied at generation level, assuring that the events would pass the level 1 trigger and therefore be recorded by the ATLAS detector.

In order to determine the ratio signal/noise, a sample of events $B \to J/\psi\ X$ was used, representing the physical background noise.

Pile-up and electronic noise were introduced at the reconstruction level as it is described in Simion's note [8].

5.3 Conditions for the analysis

For all following analysis, only the first ten electromagnetic clusters were taken into account. As the reconstruction software sorts the clusters by descending transverse energy, this doesn't cause any important data loss.

In order to obtain reconstruction efficiencies and fake rates, the reconstructed particles had to be identified with the generation data, the 'truth'. For this, the direction of the generated particle and the direction of the reconstructed one were compared. A reconstructed particle was said to be a true particle, if a generated particle satisfying

$$\angle(\vec{p}_{generated}, \vec{p}_{reconstructed}) < 2^\circ \tag{11}$$

was found. When there where more than one true particle satisfying this relation, the particle with the closest angle was selected.

5.4 Expected noise

Apart the clusters from the B_s resp. B_d decay products, a large number of clusters will be found which do not originate from the B meson to be reconstructed. First, the B meson is never created alone; even without pile-up, there are always other particles created at same time. Second, due to pile-up, a certain amount of particles not originating from the initial reaction appear.

η particles decaying into two γ...		All η			η from B_s		
$\rightarrow$	pointing to two clusters	1967	$\hat{=}$	12.7%	1809	$\hat{=}$	14.5%
	pointing to the same cluster (superimposition)	447	$\hat{=}$	2.9%	428	$\hat{=}$	3.4%
	One pointing to a cluster, one without cluster	5028	$\hat{=}$	32.4%	4765	$\hat{=}$	38.1%
	Not pointing to any cluster	8060	$\hat{=}$	52.0%	5516	$\hat{=}$	44.1%
	Total	15502			12518		

Table 1: η visibility

An important part of the latter are charged and neutral pions. The π^0 need special attention, as they decay into $\gamma\gamma$, giving clusters in the ECAL which are not easy to distinguish from the $\eta \rightarrow \gamma\gamma$ clusters. The angle between the two photons of the π^0 decay is so small that the associated clusters are next to always superimposed and identified as a single cluster by the reconstruction software.

5.5 η reconstruction for $B_s \rightarrow J/\psi\ \eta \rightarrow \mu^+\mu^-\ \gamma\gamma$

5.5.1 η visibility

The main criterium for η identification is the invariant mass of the two γ particles. Hence, for the reconstruction to be possible, two separated clusters are required. Therefore, the following two conditions have to be satisfied:

- The $\gamma\gamma$ opening angle has to be high enough ($> 5°$) so that the clusters in the EMC are not superimposed.
- The γ energies have to be sufficient ($p_T > 1\ GeV$) for the cluster to be found by the clusterization algorithm.

The ratio of η particles satisfying this two conditions gives an upper limit to the reconstruction efficiency which can be achieved by the method presented here. As shown in table 1, the maximum reconstruction efficiency that can be achieved is 14.5%. Most of the η particles get lost because the energy of at least one of the γ particles is less than $1\ GeV$.

5.5.2 Reconstruction without pile-up

The distribution of invariant mass for all possible two-cluster-pairs (figure 8) shows the eta peak above a big combinatorial background. In order to suppress this combinatorial background, we only look at the two clusters of highest transverse energy (energy deposited in presampler, samplers 1,2,3). Choosing the clusters by total energy (instead of transverse energy) was shown to give worse results (smaller efficiencies and higher fake rates). The resulting invariant mass distribution is plotted in figure 9(a). 4.0% of the η particles from B_s decays were found in an invariant mass window of $\pm 2\sigma$ around the η mass ($0.547\ GeV$[6]), but still 41% of the reconstructed η are fakes. The parameters of the gauss-fit and the obtained efficiencies are summend up in table 3 to the left. The definitions of the given numbers are given in appendix E.

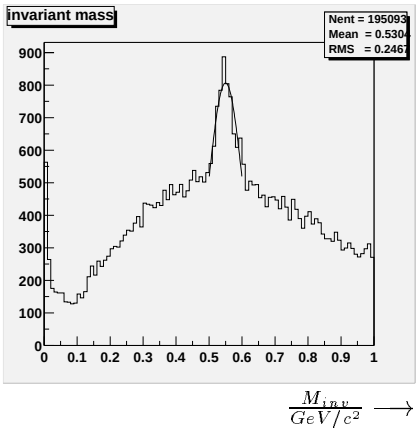

Figure 8: Two clusters invariant mass (combinatorial), no pile-up, 17039 events

η	785	$\hat{=}$	73%
π^0	46	$\hat{=}$	5%
$\pi^{\pm}$	30	$\hat{=}$	30%
γ	116	$\hat{=}$	11%
other particles and noise	102	$\hat{=}$	9%

Table 2: Origin of clusters being identified as γ from η (2σ invariant mass window)

For all following analysis, an invariant mass window of $\pm 2\sigma$ will be used.

5.5.3 Reconstruction with pile-up

With pile-up at low luminosity and electronic noise, lots of clusters not originating from η but from other particle decays appear as background noise, as can be seen in figure 9(b). As only two clusters per event are taken into account, each cluster not originating from η decay may hide an η cluster. Consequently, the reconstruction efficiency falls to 2.8%, while the fake rate remains the same. The detailed results are summed up in table 3 (right).

The peak at invariant mass zero is caused by cluster double-counting: From time to time, the same cluster is identified several times as different clusters. This peak could be eliminated by removing double-counted clusters. As this had no effect on the reconstruction efficiency and fake rate, double-counted cluster removal was not applied. The other thin peaks (most of them are only one histogram bin wide) which appeared after adding pile-up are most probably caused by problems in the pile-up algorithm.

Using the generation data, the real origins of clusters which were identified as γ from η (in the 2σ invariant mass window) were searched for. As listed up in table 2, the main contributions are coming from charged and neutral pions, photons and noise.

The task is now to suppress everything that doesn't originate from real η decays.

η reconstruction without pile-up	
$\#events$	17039
N_{η}^{gen}	20795
$N_{\eta\ from\ B_s}^{gen}$	17094
N_{η}	1164
N_{η}^{true}	684
$N_{\eta\ from\ B_s}^{true}$	676
$\epsilon(\eta\ from\ B_s)$	4.0%
f_{η}	41%
Gaussfit mean	0.551 GeV
Gaussfit σ	0.032 GeV

η reconstruction with pile-up	
$\#events$	16697
N_{η}^{gen}	20368
$N_{\eta\ from\ B_s}^{gen}$	16749
N_{η}	833
N_{η}^{true}	479
$N_{\eta\ from\ B_s}^{true}$	475
$\epsilon(\eta\ from\ B_s)$	2.8%
f_{η}	41%
Gaussfit mean	0.554 GeV
Gaussfit σ	0.039 GeV

Table 3: Reconstruction efficiencies without cuts, without and with pile-up. For the definition of the given numbers see appendix E.

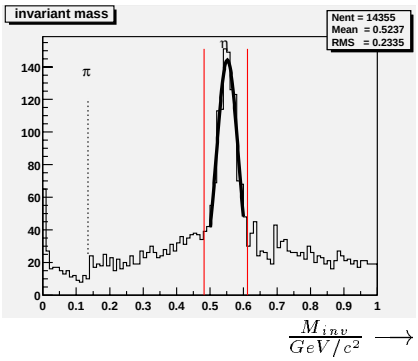

(a) no pile-up, no cuts

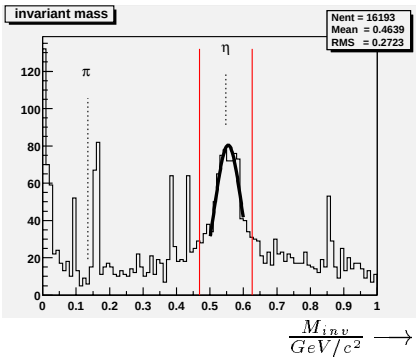

(b) with pile-up, no cuts

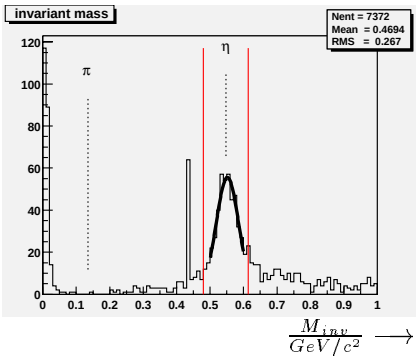

(c) with pile-up, cuts applied

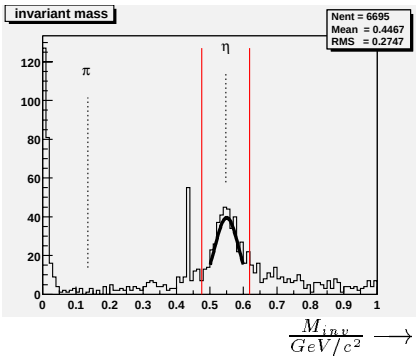

(d) with pile-up, cuts applied, with conversions

Figure 9: 2 clusters invariant mass, 2 clusters of highest p_T, with gauss fit on the η peak and $\pm 2\sigma$ invariant mass window (red)

5.5.4 Cluster rejection

Clusters originating from hadrons or noise can be identified and rejected using geometrical properties of the cluster:

- In order to reject background photons, which are situated at low p_T, and electronic noise, clusters were rejected if the transverse energy is less than $2\ GeV$. As the photons from η are also situated at rather low p_T, this cut alone reduces the η reconstruction efficiency to 2.1%.

- Clusters originating from photons are thinner than hadronic clusters, including clusters from π^0, which are the superimposition of two photons with slightly different directions. Therefore, clusters were rejected if the total cluster width, calculated using the energy deposition in 40 strips of the first sampler, is larger than 8 strips.

- In the ECAL, hadrons are not absorbed as easily as $e^{\pm}$ and γ particles. Therefore, they deposit a higher part of their energy in the third sampling of the ECAL and in the first sampling of the hadronic calorimeter. Therefore, clusters were rejected if more than 4% of the total energy is deposited in the third sampling or if more than 10% of the total transverse energy is deposited in the first sampling of the HCAL.

- Still taking profit of the difference in the cluster cross section, cuts on the energy leakage were applied: In photonic clusters, most of the energy is deposited in a 3x3 towers region in the second sampling. E_{33} being the energy deposited in this 3x3 window of the second sampling, E_{37} the energy deposited in a 3(η dir.)x7(ϕ dir) window and E_{77} the energy in a 7x7 towers window, clusters were rejected if

$$\frac{E_{37} - E_{33}}{E_{37}} > 20\% \quad \text{or} \quad \frac{E_{77} - E_{37}}{E_{77}} > 20\% \tag{12}$$

  thus demanding that the less than 20% of the energy is deposited outside the 3x3 window in both η and ϕ direction.

The concerned cluster properties are summed up in figure 10 for different cluster origins, were the differences between clusters from $\eta \to \gamma\gamma$ and other clusters are easy to see.

The cuts were applied in such a way that the first two clusters (of highest E_T) passing the cuts were combined for the η reconstruction. While the efficiency fell to 2.2%, as also some real η clusters were rejected, the fake rate could be lowered to 20%. In the obtained invariant mass distribution, as shown in figure 9(c), next to all the noise has disappeared. The detailed reconstruction results are shown in table 4.

5.5.5 $\eta \to 1$ *cluster* events

As listed up in table 1, in some of the η particle decays the $\gamma - \gamma$ opening angle is so small that the two clusters are superimposed and identified as a single cluster by the reconstruction software. As it is not possible to calculate an invariant mass for a single cluster, other η selection criteria were searched for. Using the cluster properties provided by the reconstruction software, some cuts

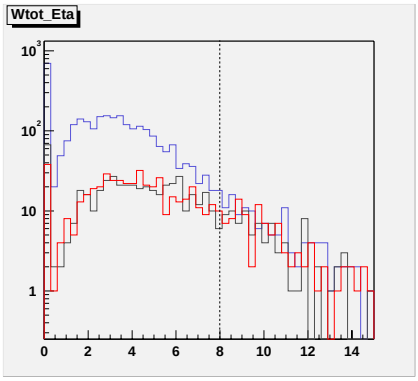

(a) Total cluster width

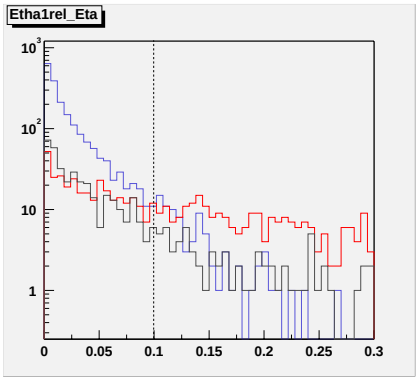

(b) $E_T(1^{st} had.sampling)/E_T$

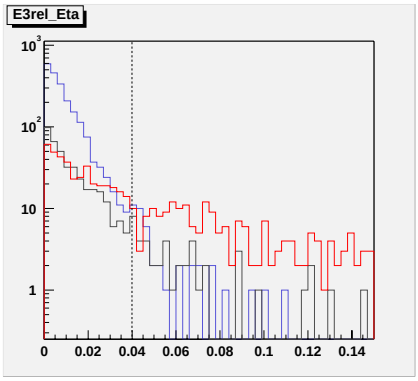

(c) $E(3^{rd} sampling)/E$

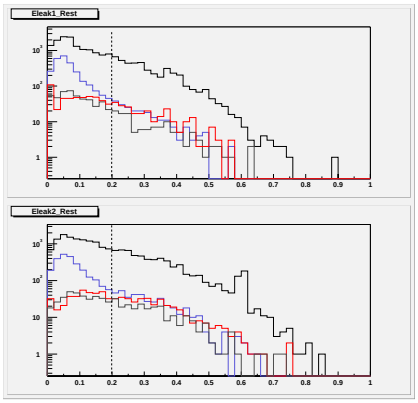

(d) Energy leakage in η(top) and ϕ direction (black: all clusters)

Figure 10: Cluster properties for clusters from η (blue), $\pi^{\pm}$ (red), π^0 (gray) and applied cuts (dashed lines). Only two clusters of highest E_T of each event.

η reconstruction with pile-up	
$\#events$	16697
N_{η}^{gen}	20368
$N_{\eta\ from\ B_s}^{gen}$	16749
N_{η}	461
N_{η}^{true}	371
$N_{\eta\ from\ B_s}^{true}$	367
$\epsilon(\eta\ from\ B_s)$	2.2%
f_{η}	20%
Gaussfit mean	0.552 GeV
Gaussfit σ	0.034 GeV

Table 4: Reconstruction efficiencies after cut application, with pile-up.

could be found which reject a certain number of non-η clusters (see appendix F). Nevertheless, the obtained fake rate was very high (85%), while the $\eta \rightarrow 1\ cluster$ efficiency was 35%, much higher than the $\eta \rightarrow 2\ cluster$ efficiency.

Due to the high fake, $\eta \rightarrow 1\ cluster$ events are not considered for the B_s reconstruction.

5.5.6 Conversions in the inner detector

In the inner detector, due to the high material density, approx. 20% of the photons convert into e^+/e^--pairs. Depending on the radius where the conversion takes place, some of the clusters from the e^+/e^- are separated (not superimposed) and deviated from the original photon direction by the applied magnetic field. In this case, the photon cannot be found using only the ECAL data. However, photon conversions can be reconstructed using inner detector tracks.

In the case of $\eta \rightarrow \gamma\gamma$, for 2.7% of the concerned photons a conversion was reconstructed, but in only 1.2% of the cases, no cluster was found in the γ direction. Consequently, adding conversions to the analysis would rise the number of photons taken into account from 36.9% to 38.2%.

Taking into account the conversions, the η from B_s efficiency slightly rised to 2.4%, whereas the fake rate changed to 23%. In fact, the conversions add more fake than real η (see appendix G).

5.5.7 B_s reconstruction and signal/noise ratio

In order to estimate the cleanliness of the B_s signal, the reconstructed η particles were combined with the J/ψ particle reconstruction as done in [5]. As the η signal after cut application was already rather clean, an invariant mass window of $\pm 5\sigma$ was used for the η selection, whereas an invariant mass window of $\pm 3\sigma$ was used for B_s reconstruction. Conversions and 1 cluster events were not taken into account.

The J/ψ reconstruction was studied under different conditions (different trigger choices). Here, only the results for the $6\ GeV/3\ GeV$ level 1 trigger were presented. This means that an event is recorded only of at least one muon with $E_T > 6\ GeV$ and a second muon with $E_T > 3\ GeV$ are present. The obtained

efficiency was

$$eff(B_s) = \frac{\#\text{reconstructed } B_s}{\#\text{ generated } B_s \text{ giving } \mu(6\ GeV)\ \mu(3\ GeV)} = \frac{386}{16288} = 2.37\% \tag{13}$$

Other than before, the reconstructed B_s particles were not identified with generated ones.

Knowing this efficiency, the number of B_s mesons which will be observed in the ATLAS detector during three years at low luminosity (the 'signal') can be calculated. As the $B_s \to J/\psi\ \eta$ branching rate is not known exactly, this was done for two different values of the branching rate: For the upper limit obtained by experiment ($3.8 \cdot 10^{-3}$ [6]) and for a theoretical prediction ($9 \cdot 10^{-4}$[7]). With this, the signal can be obtained by

$$S = \sigma_{eff}(B_s\ creation) \cdot Br(B_s \to J/\psi\ \eta) \cdot Br(J/\psi \to \mu^+\mu^-) \cdot 2 \cdot eff(B_s) \cdot L \tag{14}$$

where:

Cross section for B_s creation	$\sigma_{eff}(B_s creation)$	=	$0.251 \mu b$ [12]
Integrated luminosity	$L = \mathcal{L} \cdot 3 years$	=	$30 fb^{-1}$
$J/\psi \to \mu^+\mu^-$ branching rate	$Br(B_s \to J/\psi\ \eta)$	=	5.88%

The factor 2 in (14) expresses that B_s and $\overline{B_s}$ are involved. We get $S = 920.8 \cdot 10^6 \cdot Br(B_s \to J/\psi\ \eta) \cdot eff(B_s)$.

The same reconstruction algorithm was applied on a set of simulated $B \to J/\psi\ X$ events, where B is an arbitrary B meson decaying into J/ψ and something else. This data set represents the physics noise one will have to deal with, thus permitting to estimate how clean the signal will be, if, as in reality, the main number of events are not $B_s \to J/\psi\ \eta$ decays. The efficiency obtained was

$$eff(noise) = \frac{\#\text{ reconstructed } B_s}{\#\text{ generated } B \text{ giving } \mu(6\ GeV)\ \mu(3\ GeV)} = \frac{74}{10653} = 0.695\% \tag{15}$$

The noise is then:

$$N = \sigma_{eff}(B\ creation) \cdot eff(noise) \cdot L = 1.2 \cdot 10^8 \cdot eff(noise) \tag{16}$$

Where $\sigma_{eff}(B\ creation) = 4nb$ [14]. With this, the ratio signal/noise and the significance= $\frac{S}{\sqrt{N}}$ can be calculated:

$Br(B_s \to J/\psi\ \eta)$	$3.8 \cdot 10^{-3}$	$9 \cdot 10^{-4}$
S	$7 \cdot 10^4$	$2 \cdot 10^4$
$\frac{S}{N}$	1.48	0.35
significance $\frac{S}{\sqrt{N}}$	277	66

5.5.8 Conclusion

Without pile-up, we can easily find the η peak at $0.547\ GeV$ when calculating the two clusters invariant mass. The combinatorial background can be mostly eliminated by combining only the two clusters of highest transverse energy.

The efficiency of η reconstruction for η particles from B_s decays is 4.0%. When adding pile-up at low luminosity and electronic noise, this efficiency falls to 2.8%, due to the arrival of clusters originating from soft charged and neutral pions, as well as large amount of photons (not originating from η), small quantities of other particles (such as electrons and positrons) and electronic noise. They are also responsible for the rather huge fake rate (41%). The pions can be suppressed by applying cuts on the energy deposited in the 3^{rd} EM-sampler and the 1^{st} HCAL sampler, on the cluster width and on the energy leakages in η and ϕ directions. Electronic noise and a part of the photon contribution can be eliminated by applying a 2 GeV transverse energy cut. An η from B_s efficiency of 2.2% was achieved. The fake rate being at 20%, the signal is rather clean.

$\eta \rightarrow 1$ *cluster* events are uninteresting for the reconstruction, as the clusters cannot be easily identified.

As we are at low E_T, only few photon conversions into $e^{\pm}$-pairs were reconstructed. Consequently, adding conversions to the analysis doesn't change the reconstruction efficiency by much and gives a higher fake rate.

After having applied the reconstruction algorithm (without 1 cluster events and conversions) on the physical background, constisting of $B \rightarrow J/\psi\ X$ events, the significance of the signal, which is a measure for the cleanliness, were calculated. For the optimistic estimation of the branching rate, the obtained significance was 277, whereas for the realistic estimation still 66 was achieved. This means that the signal will be visible enough for the physical analysis.

5.6 K^{*0} reconstruction

The reconstruction of the decay channel $K^{*0} \rightarrow K^0\pi^0; K^0 \rightarrow K_s^0 \rightarrow \pi^+\pi^-$ consists of two tasks: K_s^0 reconstruction by identifying the $\pi^{\pm}$ pairs (in the inner detector) and π^0 reconstruction (in the ECAL). For this work, the focus was drawn to the π^0 reconstruction; in order to decide wether an inner detector track came from a $\pi^{\pm}$, the truth was used. Still, for the reconstruction, the measured momentums and directions were used.

5.6.1 π^0/γ separation

The $\gamma - \gamma$ opening angle of $\pi^0 \rightarrow \gamma\gamma$ decays is so small that next to all π^0 give only one cluster in the ECAL, as the clusters from the two photons are superimposed. Therefore, criteria for π^0/γ separation had to be found in a first step. In order to do this, a set of fully simulated single π^0/single γ events without electronic noise and pile-up was used and the cluster properties were analyzed and compared. The transverse energy given to the π^0's/photons was varied from 1 to 30 GeV; the transverse energy of the resulting clusters is shown in figure 11(a).

As the π^0 clusters are the superimposition of two photon clusters with slightly different directions, the following facts can be used for a differentiation:

- Cluster shape. π^0 clusters are larger than single photon clusters. For this reason, the total cluster width can be used as selection criterium.

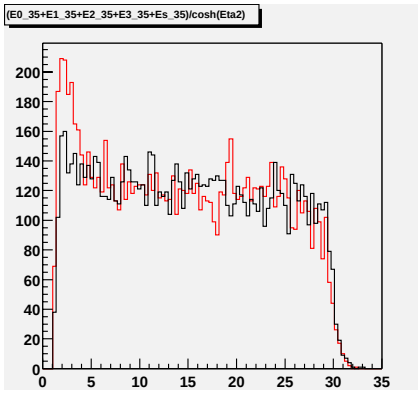

(a) Transverse energy as measured in ECAL

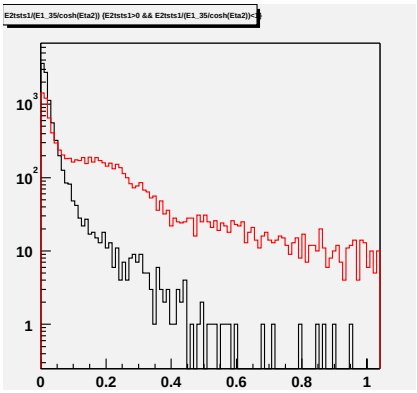

(b) $E_t(2^{nd}\ max\ in\ 1^{st}\ sampl.)/E_t(1^{st}\ sampl.)$

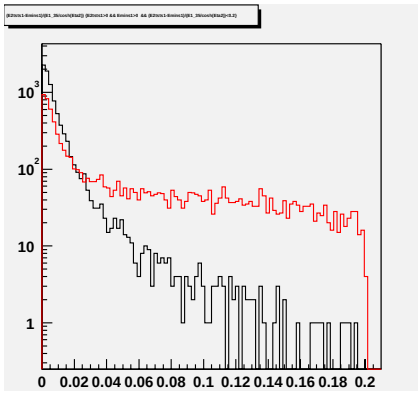

(c) $(E(2^{nd}\ max\ in\ 1^{st} sampl.) - E(min.btw.2\ maxima))/E_t(1^{st}\ sampl.)$

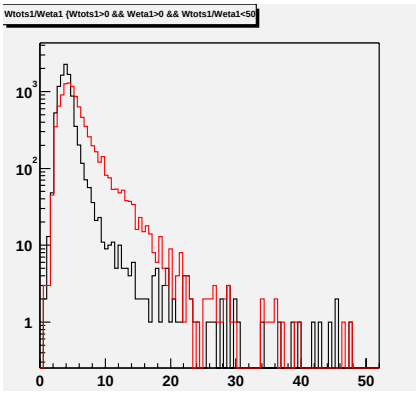

(d) Width(40 strips)/Width(3 strips)

Figure 11: Cluster properties for clusters from π^0 (red) and γ (simulated single π^0/ single γ events without pile-up)

- Second max. The first sampling of the ECAL has a high granularity in η direction. Therefore, two energy deposition maxima can be identified, corresponding to the two photons (figure 12). Useful information, such as the transverse energy of the second maximum and the minimum between the two maxima is provided by the reconstruction software and can easily be used for differentiation.

High photon rejection and acceptable π^0 efficiencies could be achieved by applying simple cuts on the mentioned cluster properties:

Cuts applied	**Surviving π^0 rate**	**Surviving γ rate**
$\frac{E2tsts1}{E1_{35}/\cosh(\eta_2)} > 0.06$ $\frac{E2ts1-Emins1}{E1_{35}/\cosh(\eta_2)} > 0.02$	45.0%	4.4%
$Wtots1 > 3$ $\frac{E2tsts1}{E1_{35}/\cosh(\eta_2)} > 0.03$ $\frac{E2ts1-Emins1}{E1_{35}/\cosh(\eta_2)} > 0.015$ $Emins1/E1_{35} > 0.01$ $E2ts1/E1_{35} > 0.02$	22.8%	2.9%

Where the variables have the following meanings:

$E2tsts1$	Transverse energy of 2nd max (1 strip) in first sampling
$E2ts1$	Transverse energy of 2nd max (3 strips) in first sampling
$Emins1$	Energy minimum between two maxima in first sampling
$Wtots1$	Total cluster width (over 40 strips)
$E1_{35}$	Energy in first sampling (3x5 cell)
η_2	Pseudorapidity as measured in second sampling
$Weta1$	Cluster width (over 3 strips)

5.6.2 π^0 selection

In order to find the π^0 coming from the K^{*0} decay, the ECAL cluster of highest p_T which passes the chosen cuts was selected. Compared to the π^0 studied above, the π^0 concerned here are at lower transverse momentum, and the cuts presented above appear to be next to useless. Additionally, the π^0 we are looking for are energetically rather close to the pile-up, see figure 13(a), wich makes the search even more difficult.

Figure 13(b) shows the correlation between generated and reconstructed transverse momentum: They match within an acceptable range.

The cluster rejection was optimized in order to obtain the lowest possible fake rate. Table 5 shows the applied cuts and the efficiency after cut application: The achieved π^0 from K^{*0} efficiency was 9.0%, while the fake rate was at 73%.

The cuts were found by using a simple search algorithm which finds the cut value giving the minimal fake rate, provided that not more than 70% of real

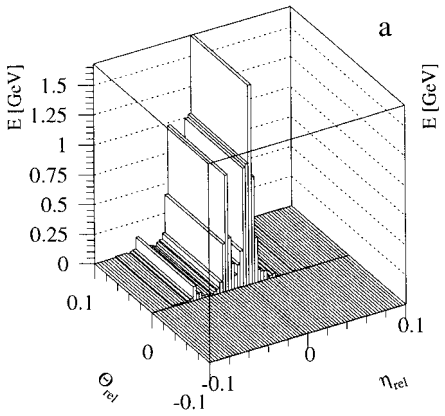

Figure 12: Substructure of a hadronic cluster in the 1^{st} sampling [9]: Two energy maxima are visible

Cuts for π^0 from K^{*0} selection				
		E_T	$>$	2.5 GeV
		$\frac{E_{37}-E_{33}}{E_{37}}$	$>$	0.02
1.8	$<$	$Wtots1$	$<$	7.8
0.04	$<$	$\frac{E2tsts1}{E_{35}/\cosh(\eta_2)}$	$<$	1.44
3.2	$<$	$\frac{Wtots1}{Weta1}$	$<$	16.8
		$\frac{E2tsts1-Emins1}{E_{35}/\cosh(\eta_2)}$	$>$	0.016

π^0 selection with pile-up	
$\#events$	9016
$N^{gen}_{\pi^0}$	60104
$N^{gen}_{\pi^0\ from\ B_d \to J/\psi K^{*0}}$	8963
N_{π^0}	4811
$N^{true}_{\pi^0}$	1300
$N^{true}_{\pi^0\ from\ B_d \to J/\psi K^{*0}}$	805
$\epsilon(\pi^0\ from\ B_d \to J/\psi K^{*0})$	9%
f_η	73.0%

Table 5: π^0 from K^{*0} reconstruction: Applied cuts (left) and efficiencies (right). The meanings of the variables are listed up on page 23.

π^0 are rejected. The cuts slightly improve the π^0 fake rate, but the π^0 from $K^{*0}(B_d)$ efficiency has dropped. In both cases, approximately the same amount of the real reconstructed π^0 (38%) is not coming from K^{*0} decays.

5.6.3 K^0_S reconstruction

For the $K^0_S \to \pi^+\pi^-$ reconstruction, inner detector tracks were used for $\pi^\pm$ reconstruction.

Three approaches were made in order to reconstruct the K^0_S particles. In all three cases, the truth (data from generation) was used in order to decide wether an inner detector track is coming from a $\pi^\pm$. However, for the reconstruction, the momentum measured by the inner detector was used. In all three cases, inner detector tracks with a fit parameter $\chi^2 > 6$ were rejected.

1. **For reference: Use the truth.** Using the data from generation, the $\pi^\pm$-pairs coming from the $K^0_S(B_d \to K^{*0})$ decays were searched for. Consequently, the K^0_S fake rate is practically ≈ 0. The K^0_S from $K^{*0}(B_d)$ efficiency was at 31%.

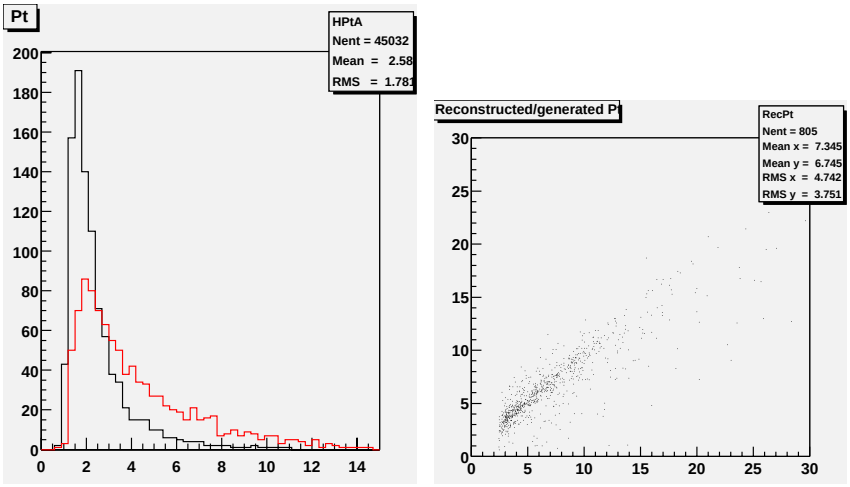

(a) p_T of π^0 from K^{*0} (red) and other clusters. Both curves are normalized to 1000.

(b) p_T from generation (x axis) and reconstructed p_T (y axis) for π^0 from K^{*0}

Figure 13: π^0 from K^{*0} p_T from generation and reconstruction

2. **Select $\pi^{\pm}$ with highest p_T.** In this approach, the π^+ and π^- tracks of highest p_T were (independently) selected and combined. Under this somewhat more realistic conditions, the efficiency dropped down to 2.2%, while the fake rate jumped to 80%, due to a great number of pions originating from pile-up. As shown in table 6 to the upper left, the gauss fit mean value is far away from the K_S mass. Therefore, this method can be said to be not advisable.

3. **Select $\pi^{\pm}$ with best invariant mass.** Finally, each π^+ was combined with each π^-, and the combination giving the best invariant mass (closest to the K^0 mass) was chosen. This rises the fake rate to 85%, but the efficiency (11.1%) is more than five times as high as with method 2.

The detailed results of K^0_S reconstruction using the three methods are summed up in table 6. As before, an invariant mass window of $\pm 2\sigma$ was used for all analysis. The invariant mass distributions are shown in figure 14 (a)-(c). The K^0_S reconstruction done here was made only to obtain the order of magnitude of the K^{*0} reconstruction efficiency; an optimized K^0_S reconstruction using vertexing was done in [10].

5.6.4 K^{*0} reconstruction

The last step is to combine the reconstructed K^0_S with the π^0 particles in order to reconstruct the K^{*0} particle. The best results were obtained by combining the best invariant mass method for the K^0_S with the cuts for the π^0 as described above; The $K^0_S - \pi^0$ invariant mass distribution is shown in figure 14(d); the

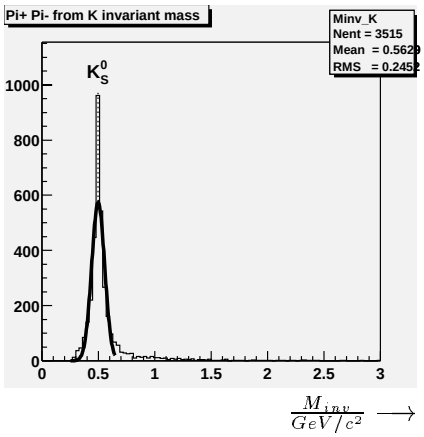

(a) $\pi^+ - \pi^-$ invariant mass: Using the truth

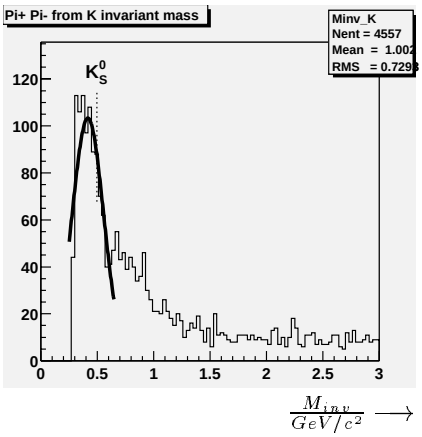

(b) $\pi^+ - \pi^-$ invariant mass: $\pi^{\pm}$ with highest p_T

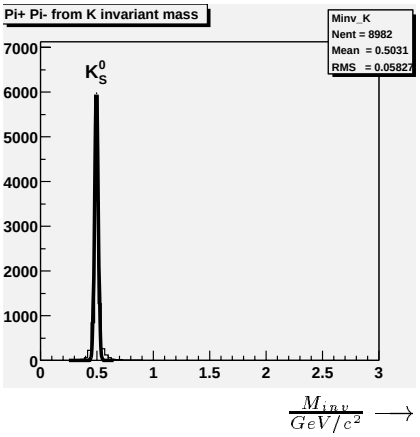

(c) $\pi^+ - \pi^-$ invariant mass: $\pi^{\pm}$ with best invariant mass

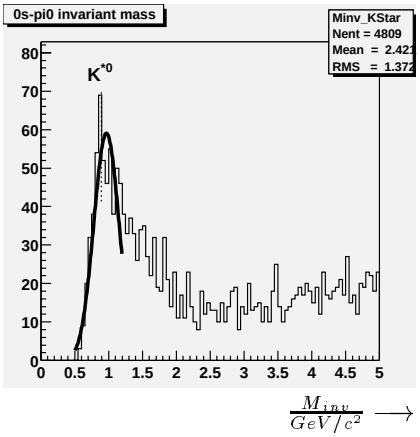

(d) $K^0_S - \pi^0$ invariant mass

Figure 14: K^0_S and K^{*0} reconstruction

K^0_S reconstruction with pile-up	
$\#events$	9016
$N^{gen}_{K^0_S}$	15357
$N^{gen}_{K^0_S\ from\ B_d}$	9016
Using the truth	
$N_{K^0_S}$	2801
$N^{true}_{K^0_S}$	2787
$N^{true}_{K^0_S\ from\ B_d}$	2787
$\epsilon(K^0_S\ from\ B_d)$	31%
$f_{K^0_S}$	0.5%
Gaussfit mean	0.499 GeV
Gaussfit σ	0.057 GeV

$\pi^{\pm}$ with highest p_T	
$N_{K^0_S}$	1196
$N^{true}_{K^0_S}$	239
$N^{true}_{K^0_S\ from\ B_d}$	202
$\epsilon(K^0_S\ from\ B_d)$	2.2%
$f_{K^0_S}$	80%
Gaussfit mean	0.418 GeV
Gaussfit σ	0.139 GeV
$\pi^{\pm}$ with best invariant mass	
$N_{K^0_S}$	7558
$N^{true}_{K^0_S}$	1131
$N^{true}_{K^0_S\ from\ B_d}$	998
$\epsilon(K^0_S\ from\ B_d)$	11.1%
$f_{K^0_S}$	85%
Gaussfit mean	0.497 GeV
Gaussfit σ	0.016 GeV

Table 6: $K^0_S \to \pi^+\pi^-$ reconstruction

K^{*0} reconstruction with pile-up	
$\#events$	9016
$N^{gen}_{K^{*0}\ from\ B_d}$	9016
$N_{K^{*0}}$	510
$N^{true}_{K^{*0}}$	128
$N^{true}_{K^{*0}\ from\ B_d}$	126
$\epsilon(K^{*0}\ from\ B_d)$	1.4%
$f_{K^{*0}}$	75%
Gaussfit mean	0.968 GeV
Gaussfit σ	0.168 GeV

Table 7: K^{*0} reconstruction; with pile-up; K^0_S reconstruction using the best invariant mass method; π^0 selection after cut application.

reconstruction results are listed up in table 7. The obtained efficiency with this method was 1.4% with a fake rate of 75%.

5.6.5 Signal/noise ratio

Yet, no B_d reconstruction was done, but anyhow an upper limit to the signal/noise ratio and the significance can be given. It was assumed that by combining with the reconstructed J/ψ particles, all fake K^{*0} can be eliminated. Therefore, only real K^{*0} particles (those which were identified to generated ones) were counted. Additionnally, it was assumed that the J/ψ particles can be reconstructed with an efficiency of 100% and no fakes. In analogy to the equations (14) and (16) on page 20, the number of signal and noise events was calculated using

Cross section for B_d creation	$\sigma_{eff}(B_d\ creation)$	=	$0.214\mu b$ [13]
Integrated luminosity	$L = \mathcal{L} \cdot 3\ years$	=	$30fb^{-1}$
$B_d \to J/\psi\ K^{*0}$ branching rate	$Br(B_d \to J/\psi\ K^{*0})$	=	$1.5 \cdot 10^{-3}$ [6]
K_S^0 part in K^0	$Br(K^0 \to K_S^0)$	=	0.5

For the efficiencies, the values obtained by combining the K_S reference method (using the truth) and π^0 selection using the cuts were used: $\epsilon(K^{*0} from B_d) = 3\%$. For the noise estimation, the same set of simulated $B \to J/\psi\ X$ events as before was used and the efficiency was $6 \cdot 10^{-4}$. The upper limits to signal/noise and significance obtained were:

signal S	$\tilde{<}$	$1.62 \cdot 10^4$
$\frac{S}{N}$	$\tilde{<}$	0.2
significance $\frac{S}{\sqrt{N}}$	$\tilde{<}$	58

5.6.6 Conclusion

Whereas π^0/γ-distinction appears not to pose big problems at higher transverse momentum, no effective distinction criterium could be found which could have helped to identify the neutral pions from K^{*0} decays. Some cuts were found which slightly improve the fake rate but which reject also many real π^0 particles. The cuts had the same impact on the K^{*0} reconstruction: The fake rate dropped by some percent, but a great amount of K^{*0} was lost, too. The following table gives a short overview of the K^{*0} efficiencies obtained by the different methods:

π^0 **selection**	K_S^0 **reconstruction**	$K^{*0}(B_d)$ **efficiency**	K^{*0} **fake rate**
no cuts	using the truth	5.0%	12.1%
no cuts	$\pi^+ - \pi^-$ of highest p_T	1.1%	77.7%
no cuts	best inv. mass	2.2%	76.9%
cuts applied	using the truth	3.0%	11.1%
cuts applied	$\pi^+ - \pi^-$ of highest p_T	0.7%	74.4%
cuts applied	best inv. mass	1.4%	74.9%

It appears that the K^{*0} reconstruction could still be rescued by a better K_S^0 reconstruction method, as the K^{*0} fake rate is at a rather low level if the truth is used for the K_S^0, even if the π^0 fake rate is very high. In addition, a big part of the K^{*0} should possibly be suppressed if the combination with the J/ψ particle is done in order to reconstruct the B_d meson.

Making this rather optimistic assumption, the upper limit to the signal significance was ≈ 58. Hence, the signal will be less clean than for the $B_s \to J/\psi\ \eta$ decay channel. Nevertheless, this will probably be sufficient.

6 Conclusion

The goal of this work was to find out wether two specific B meson decay channels, which will permit precision measurements in the domain of CP violation, will give a visible and sufficiently clean signal in the ATLAS detector at LHC. For the first of them, $B_s \rightarrow J/\psi\ \eta$, the answer can now be given: Yes. Even if electronic noise, pile-up and the physical background ($B_s \rightarrow J/\psi\ X$) are taken into account, the obtained signal/noise ratio indicates that the signal will be clean enough for the desired measurements.

For the second decay channel which was analyzed, $B_d \rightarrow J/\psi\ K^{*0}$, the answer should be 'probably, yes'. Making rather optimistic assumptions on the fake K^{*0} rejection which could be achieved, an upper limit to the signal/noise ratio could be given, indicating that the signal will be somewhat less clean than in the case of $B_s \rightarrow J/\psi\ \eta$. Still, the given limit is high enough so that there is still hope that the decay channel could be used for the desired CP violation measurements. To obtain clearer results, the π^0 selection has still to be improved, and the K^0_S reconstruction has to be done properly, as proposed in [10], where a K_S reconstruction efficiency of 41% was achieved. Additionnally, the combination with the J/ψ particle has to be done in order to reconstruct the B_d meson.

References

[1] ATLAS calorimeter performance, technical design report, CERN-LHCC/96-40

[2] B decays at the LHC, CERN-TH/2000-101

[3] CP Violation in B Decays and Strategies for Extracting CKM Phases, CERN-TH/98-288, hep-ph/9809216

[4] Quark Mixing and CP Violation, hep-ph/9800230

[5] J/ψ reconstruction in the inner detector, S. Viret: *http://isnwww.in2p3.fr/atlas/fairouz/physics/viret/index.html* and rapport de stage DEA, matière et rayonnement, 2001.

[6] Review of Particle Physics, Europ. Phys. Journ. C15, (2000) 1-4

[7] P.Z. Skands, Int. J. High Energy Phys. 0101 (2001) 8, hep-ph/0010115

[8] S.Simion, Atlas note: ATL-SOFT-99-001

[9] M.Wielers, Atlas note: ATL-PHYS-99-016

[10] K_S^0 reconstruction in the ATLAS Inner Detector, J. Damet, G.F. Tartarelli; ATL-INDET-99-024

[11] J.P. Jessop et al. (CLEO Collaboration), Phys. Rev. Lett. 79, 4533 (1997)

[12] PYTHIA calculations on the cross section of B_s creation, *http://isnwww.in2p3.fr/atlas/fairouz/physics/bsjpsieta/X_section*

[13] PYTHIA calculations on the cross section of B_d creation, *http://isnwww.in2p3.fr/atlas/fairouz/physics/bdjpsik0star/ftn55*

[14] PYTHIA calculations on the cross section of B creation, *http://home.cern.ch/m̃smizans/production/datacards/atgenAug97/Jpsimumu/Xsection.html*

A The role of symmetries

A.1 Types of symmetries

Two types of symmetries can be differentiated

- **Continuous symmetries.** These are symmetries under transformations that can be composed of infinitely small transformations, as for example:
  - Symmetry under translation, leading to impulse conservation
  - Symmetry under rotation, leading to conservation of angular momentun
  - Gauge symmetry in QED, leading to charge conservation
- **Discrete symmetries.** The symmetry transformation involved cannot be composed of smaller transformations. Among them:
  - Parity (**P**): Mirror symmetry
  - Charge conjugation (**C**): Symmetry under replacement of all particles by the corresponding antiparticles
  - Time inversion (**T**): Determines wether a process can be reversed

In quantum mechanics, the symmetry operations C, P and T are represented by operators acting on the physical states. As $P^2 = C^2 = T^2 = \mathbb{1}$, the only possible eigenvalues of each and of all combinations are ± 1.

A.2 Discrete symmetries

A.2.1 P symmetry

The operator P performs a reflection of all three space coordinates

$$\langle \vec{r}| P |\Psi\rangle = \langle -\vec{r}|\Psi\rangle \tag{17}$$

which is equivalent to a reflection of one axis and a rotation of 180°.

P symmetry was introduced by Wigner in order to explain the two types of excitated states of atoms wich were observed by Laporte in 1924. Since then it was held up as a basic principle, until its refutation by the experiment of Wu. Maximal P violation was found in the nuclear decay of ^{60}Co which is governed by the weak interaction.

A.2.2 C symmetry

By the C operation, particles are replaced by the corresponding antiparticles and vice versa.

While the charge seems to be the only difference between matter and antimatter, also the C symmetry was found to be maximally violated by weak interaction. This C violation is closely related to the P violation mentioned above.

A.2.3 CP symmetry

The fact that both P and C symmetry are violated by weak interaction makes it interesting to take a look at their combination. In fact, it appears that CP holds in the processes mentioned above, which means that antimatter behaves exactly like matter, if one looks at it in the mirror.

Nevertheless, in 1964 a small CP violation effect was found in Kaon decays, implying that nature indeed makes a small difference between matter and antimatter.

A.2.4 Time reversal

The action of the T operation consists principally in reflecting the impulsion of all particles. T symmetry means that all physical processes are the same, wether the time runs forward or backward. But attention! This has nothing to do with the fact that one sees more often how a glass is breaking than small pieces which organize themselves to reassemble the glass. This is a pure statistical effect, as the number of states 'pieces on the floor' is incountable, as opposed to one single state 'glass on the table'.

A.2.5 The CPT theorem

While the P and CP symmetries were introduced and demanded for reasons of beauty and simplicity, it can be derived from the basic principles of physics (locality, causality etc.), that the combination CPT has to be conserved. This means for example that, if CP is violated, there must also be a compensating violation of T symmetry, meaning that there is a fundamental sense of time, distinguishing the future from the past.

Nevertheless, it is to note that the CPT theorem may possibly be doubted in string theory, where locality does no longer apply.

B B physics experiments

Due to the big interest in B physics, several experiments specially dedicated to this domain were constructed.

- In the past, CDF-run I at Fermilab and LEP experiments at CERN already collected data which can be used for B physics.
- Presently, accelerator systems specially dedicated to B physics, so-called 'B fabrics', are at work:
  - BaBar at SLAC
  - Belle in Japan
- In the near future, the LHCb detector will, as ATLAS, analyze proton-proton collisions at LHC. LHCb is specially dedicated to B physics and thus far less complex than ATLAS.
- Also in the near future, a second run of CDF will provide additional data.

Additionally, there are some experiments for K physics studies, as:

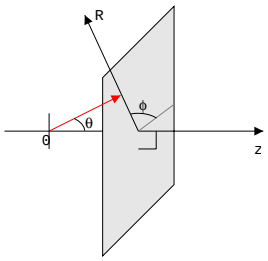

Figure 15: Coordinate system

- NA48 at CERN
- KTEV at SLAC

While most of the B experiments are constructed in order to explore B physics qualitatively and hopefully find new physics, B physics at LHC provides the following advantages:

- Even at low luminosity, huge amounts of B mesons will be created. This leads to better statistics, so that precision measurements of the CP violation parameters are possible.
- Due to the center-of-mass energy of 14 TeV, the heavier B_s mesons can be created, whereas BaBar/Belle operate just above the B_d theshold.

C Coordinate system

In order to describe the interactions, a coordinate system as presented in figure 15 is used, where z is the beam axis, and $z = 0$ corresponds to the interaction point. Instead of the angle θ, usually the pseudorapidity η is used, being defined as

$$\eta = -\ln \tan \frac{\theta}{2} \tag{18}$$

Often, instead of the total momentum or energy, only the component in the $R - \phi$ plane is used, as all distributions are independant of the longitudinal momentum. The transverse momentum p_T and transverse energy E_T are thus defined as

$$E_T = \frac{E}{\cosh \eta} \tag{19}$$

$$p_T = \frac{p}{\cosh \eta} \tag{20}$$

Given the transverse momentum, η and ϕ, the momentum vector can be obtained by

$$\vec{p} = \begin{pmatrix} p_T \cos \phi \\ p_T \sin \phi \\ p_T \sinh \eta \end{pmatrix} \tag{21}$$

D Simulation

In order to analyse the capabilities of the ATLAS detector, a simulation software was written, which generates signals as will be obtained by the real detector later, taking into account all known physics effects. The simulation takes place in several steps:

1. The proton-proton collision and the following particle interactions and reactions are simulated. At this level, specific reactions and decay channels can be forced to take place. Also at generation level, cuts on particle directions and energies can be applied, in order to obtain only events which will be observed by the virtual ATLAS detector and thus to economize calculation time.

2. The reaction is placed into the detector and the impact of the detector material is calculated in detail. As a large amount of particles is created in the electromagnetic and hadronic showers, this simulation step demands much calculation time ($\approx$ 20 minutes per event on a Linux PC). The electronic signals obtained at the end of each calorimeter region are calculated.

3. If desired, electronic noise and pile-up are added. For pile-up, a certain number of minimum-bias events is added to the event, taking into account the detector geometry.

4. The signals obtained are passed to the reconstruction software that will also be used on the real detector signal later. Inner detector tracks are reconstructed, clusterization is done and cluster and track properties are stored for later use.

5. The last step consists of the search for and reconstruction of the desired particles.

E Definitions: Efficiency and fake rate

The main criteria for judging the reconstruction quality are the reconstruction efficiency and fake rate, defined as follows:

- N_X: Number of reconstructed X particles
- N_X^{true}: Number of reconstructed X particles associated to a generated X particle
- N_X^{fake}: Number of reconstructed X particles not associated to a generated X particle;

$$N_X = N_X^{true} + N_X^{fake} \tag{22}$$

- N_X^{gen}: Number of generated X particles
- $N_{X\ from\ Y}^{true}$: Number of reconstructed particles associated to a generated X particle belonging to the decay channel Y

- $N^{gen}_{X\ from\ Y}$: Number of generated X particles belonging to the decay channel Y
- Overall X reconstruction efficiency:

$$\epsilon(X) = \frac{N^{true}_X}{N^{gen}_X} \tag{23}$$

- X from Y efficiency

$$\epsilon(X\ from\ Y) = \frac{N^{true}_{X\ from\ Y}}{N^{gen}_{X\ from\ Y}} \tag{24}$$

- fake rate

$$f_X = \frac{N^{fake}_X}{N_X} \tag{25}$$

F $\eta \to 1\ cluster$ events

In order to identify clusters which are the superimposition of the two clusters from $\eta \to \gamma\gamma$, the following cuts were applied:

- The transverse energy has to be at least 10 GeV. This rejects most of the pile-up clusters. As the clusters now contain the energy of both γ particles, the typical cluster energy is much higher than in 2 cluster decays.
- The total cluster width (over 40 strips) has to be between 2 and 9 strips. It was shown that most of the η clusters have a width within this window.
- Due to the high pseudorapidity resolution in first sampling, two energy maxima are found corresponding to the two γ, enclosing an energy minimum in between. Clusters were rejected, if this energy minimum is more than 0.4% of the total transverse energy.
- Because of the non rotational symmetric shower shape, the energy leakage in η and ϕ direction are correlated. Clusters were rejected, if $(E_{37} - E_{33})/E_{37} > 15\%\ and\ (E_{77} - E_{37})/E_{77} > 15\%$. Also, clusters were rejected if $(E_{37} - E_{33})/E_{37} > 50\%\ or\ (E_{77} - E_{37})/E_{77} > 50\%$

These cuts were chosen after a comparative analysis of the cluster properties, showing that the typical η clusters would pass the cuts. The obtained efficiencies are:

$\eta \to 1\ cluster$ reconstruction with pile-up	
$\#events$	16697
N^{gen}_{η}	20368
$N^{gen}_{\eta\to 1\ cluster}$	477
$N_{\eta\to 1\ cluster}$	1073
$N^{true}_{\eta\to 1\ cluster}$	166
$\epsilon(\eta \to 1\ cluster)$	35%
$f_{\eta\to 1\ cluster}$	85%

Here (and only here), for the η identification with the truth, the cluster energy was forced to be within a window of $\pm 30\%$ around the generated η particle energy. As before, the direction of cluster and generated particle had to match within 2°.

Reconstruction efficiency and fake rate were not affected by pile-up, because the cluster energies are now superior to the energies of clusters coming from pile-up.

G Conversions in the inner detector in the case of $\eta \to \gamma\gamma$

Counting only photons from the decay channel $B_s \to J/\psi\ \eta;\ \eta \to \gamma\gamma$, the following number of reconstructed photon conversions were found:

$\#events$	16679		
$\#\gamma$	25370		
$\#\gamma \to 1\ cluster$	9369	$\hat{=}$	36.9%
# converted γ	675	$\hat{=}$	2.7%
# converted γ, still giving 1 cluster	361	$\hat{=}$	1.4%
# converted γ, no cluster in γ dir.	314	$\hat{=}$	1.2%

The algorithm used to take into account the conversions for the η reconstruction tries the following combinations, until an invariant mass within the $\pm 2\sigma$ is found:

1. Two ECAL clusters of highest E_T
2. ECAL cluster of highest E_T and conversion of highest p_T
3. Two conversions of highest p_T

In order to suppress fake conversions, conversions were rejected if the fit parameter (quality) χ^2 was superior to 5. Cluster rejection was not changed.

Taking into account the conversions, the η from B_s efficiency slightly rised to 2.4%, whereas the fake rate changed to 23%.